EBioMedicine 9 (2016) 180–194

Contents lists available at ScienceDirect

EBioMedicine

journal homepage: www.ebiomedicine.com

Research Paper

Histidine-Rich Glycoprotein Prevents Septic Lethality through Regulation of Immunothrombosis and Inflammation

Hidenori Wake [a], Shuji Mori [f], Keyue Liu [a], Yuta Morioka [a], Kiyoshi Teshigawara [a], Masakiyo Sakaguchi [b], Kosuke Kuroda [c], Yuan Gao [a], Hideo Takahashi [g], Aiji Ohtsuka [d], Tadashi Yoshino [e], Hiroshi Morimatsu [c], Masahiro Nishibori [a,*]

[a] Department of Pharmacology, Okayama University Graduate School of Medicine, Dentistry, and Pharmaceutical Sciences, Okayama 700-8558, Japan
[b] Department of Cell Biology, Okayama University Graduate School of Medicine, Dentistry, and Pharmaceutical Sciences, Okayama 700-8558, Japan
[c] Department of Anesthesiology and Resuscitology, Okayama University Graduate School of Medicine, Dentistry, and Pharmaceutical Sciences, Okayama 700-8558, Japan
[d] Department of Human Morphology, Okayama University Graduate School of Medicine, Dentistry, and Pharmaceutical Sciences, Okayama 700-8558, Japan
[e] Department of Pathology, Okayama University Graduate School of Medicine, Dentistry, and Pharmaceutical Sciences, Okayama 700-8558, Japan
[f] Department of Pharmacology, Shujitsu University, School of Pharmacy, Okayama 703-8516, Japan
[g] Department of Pharmacology, Kinki University, Faculty of Medicine, Osakasayama 589-8511, Japan

ARTICLE INFO

Article history:
Received 4 April 2016
Received in revised form 2 June 2016
Accepted 2 June 2016
Available online 4 June 2016

Keywords:
Histidine-rich glycoprotein
Sepsis
ARDS
Immunothrombosis
Neutrophil

ABSTRACT

Sepsis is a major cause of death worldwide. We show that a plasma protein histidine-rich glycoprotein (HRG) was decreased significantly in septic mice with cecal ligation and puncture (CLP) and supplementary treatment of septic mice with exogenous HRG improved survival, with strong inhibition of tight attachment of neutrophils to pulmonary vasculatures, subsequent immunothrombosis, DIC state, lung inflammation, hypercytokinemia, and activation of vascular endothelial cells (VECs). In contrast, knockdown of HRG by siRNA exacerbated lethality. Purified human HRG reversibly induced morphological changes in human neutrophils *in vitro*; induction of spherical shape with reduced microvilli and adhesiveness to VECs. HRG maintained the passage of neutrophils through microcapillaries and abolished production of reactive oxygen species. These results suggested that the supplementary therapy with HRG may provide a novel strategy for the treatment of sepsis through suppression of excessive systemic inflammation and immunothrombosis by keeping circulating neutrophils quiescent and preventing uncontrolled activation of VECs.

1. Introduction

Sepsis is a systemic inflammatory response syndrome (SIRS) associated with infection. The pathogenesis of sepsis includes the disturbance of blood-vascular homeostasis, which may cause multiple organ failure, circulatory shock, and disseminated intravascular coagulation (DIC), leading to high mortality (Aziz et al., 2013; Dellinger et al., 2012; Hotchkiss et al., 2013; Semeraro et al., 2012). The proinflammatory cytokine response in the acute phase may be triggered by the constituents of invading pathogens and tissue damage-associated molecular patterns (Piccinini and Midwood, 2010; Ward, 2012), accompanied by the activation of vascular endothelial cells (VECs), a pivotal step for inducing the migration of leukocytes into inflammatory sites with pathogen invasion (Salomão et al., 2008; Williams et al., 2011). A recent study suggested that neutrophil adhesion on VECs may trigger platelet aggregation and immunothrombus formation in septic acute respiratory distress syndrome (ARDS) (Grommes and Soehnlein, 2011; Matthay and Zemans, 2011; Moreland et al., 2004; Engelmann and Massberg, 2013; Brinkmann et al., 2004; Yipp and Kubes, 2013). Thus, circulating neutrophils may play important roles in the pathogenesis of septic conditions in addition to infiltrating neutrophils. However, the uncontrolled activation of neutrophils has not been examined in detail due to methodological limitations (Alves-Filho et al., 2008). Neutrophils are easily activated by *in vitro* handling or even by withdrawing from blood vessels. Therefore, it might be rather difficult to know and speculate about the precise features of the circulating neutrophils by an *in vitro* analysis. Also, if any are present, a controlling factor of neutrophils in plasma, one that might regulate a fundamental state of circulating neutrophils in both healthy and disease conditions, remains to be determined.

Histidine-rich glycoprotein (HRG) is a 75 kDa plasma glycoprotein produced in and secreted from the liver (Koide et al., 1986). The plasma levels of HRG in healthy human were reported to be constant around 1 μM (Poon et al., 2011). HRG's primary amino acid sequence has an extraordinary number of histidine residues and typical GHHPH repeats (Borza et al., 1996). Since HRG binds to a diverse range of ligands including heparin, heparan sulfate, fibrin, fibrinogen, plasminogen,

* Corresponding author.
E-mail address: mbori@md.okayama-u.ac.jp (M. Nishibori).

http://dx.doi.org/10.1016/j.ebiom.2016.06.003

thrombospondin, divalent metal cations, heme, and complement C1q, it is suggested to be involved in the regulation of coagulation/fibrinolysis (Lijnen et al., 1983; Leung, 1986; Peterson et al., 1987; Silverstein et al., 1985), immune response (Gorgani et al., 1997; Morgan, 1985; Poon et al., 2010), and angiogenesis (Doñate et al., 2004; Juarez et al., 2002; Wake et al., 2009). Moreover, HRG is reported to have the antibacterial and antifungal activities in acidic pH and high Zn condition (Rydengård et al., 2007; Kacprzyk et al., 2007; Rydengård et al., 2008) as well as the neutralizing effect on lipopolysaccharide (LPS) (Bosshart and Heinzelmann, 2003). Actually, Shannon et al. demonstrated that HRG decreases mortality of septic mice model with *S. pyogenes*-induced abscess by killing and trapping of bacteria in abscess site (Shannon et al., 2010). However, the effects of HRG on the circulating leukocytes, especially neutrophils in systemic septic condition, are poorly understood.

In the present study, we identified and characterized HRG as a unique plasma factor that maintains a neutrophil's spherical shape with minimal microvilli on the surface independent of the extravascular action. These morphological features render neutrophils quiescent with respect to the cell adhesion to VECs, the passage of microvasculatures, and the spontaneous release of reactive oxygen species (ROS). In cecal ligation and puncture (CLP) sepsis mice, plasma levels of HRG decreased significantly, and supplementary treatment with human HRG dramatically improved the survival rate of CLP mice associated with the inhibition of immunothrombosis in pulmonary vasculatures, DIC state, hypercytokinemia, and inflammatory responses in the lung, without interfering with the infiltration of neutrophils into the peritoneal cavity. The present study has shed light on our understanding of septic conditions by clarifying a crucial role of HRG in neutrophils.

2. Materials and Methods

2.1. Reagents

Thrombin (from human plasma), isoluminol, and horseradish peroxidase type IV were obtained from Sigma (St. Louis, MO). DAPI, SYTOX Blue, SYTOX Green, Hoechst33342, Calcein-AM, Fluo-4, CM-H2DCFDA, Phalloidin-Alexa584, DNaseI-Alexa488, BAPTA-AM, and Invivofectamine were obtained from Life Technologies (Carlsbad, CA). Anti-phosphatidylserine antibody (Ab) (clone: 1H6) were obtained from Merck (Darmstadt, Germany). *N*-formyl-*L*-methionyl-*L*-leucyl-phenylalanine (fMLP) was obtained from Peptide Institute, Inc. (Minoh, Japan). Toxin B from *Clostridium difficile* was obtained from List Biological Laboratories (Campbell, *CA*). Imipenem (TIENAM for intramuscular injection) was obtained from MSD (Tokyo, Japan). C5a, IL-8, anti-mouse myeloperoxidase (MPO) Ab, and anti-mouse CD42d Ab were obtained from R&D systems (Minneapolis, MN). Anti-mouse fibrinogen/fibrin Ab, anti-Histone H3 Ab (citrulline R2 + R8 + R17) (cit-histone H3), DyLight488-labeled anti-human CD54 Ab (clone: EPR4776), Alexa Fluor 647-labeled anti-rabbit IgG Ab, Alexa Fluor 647-labeled anti-sheep IgG Ab, Alexa Fluor 568-labeled anti-rabbit IgG Ab, Alexa Fluor 568-labeled anti-sheep IgG Ab, Alexa Fluor 568-labeled anti-goat IgG Ab, Alexa Fluor 488-labeled anti-goat IgG Ab, and Alexa Fluor 405-labeled anti-rabbit IgG Ab were obtained from abcam (Cambridge, UK). FITC-labeled anti-human activated CD11b Ab (clone: CBRM1/5) were obtained from eBioscience (San Diego, *CA*). Alexa Fluor 488-labeled anti-human CD62P Ab was obtained from BiossAntibodies (Woburn, MA). Anti-mouse Gr-1 (clone: RB6-8C5)-Alexa Fluor 594 was obtained from BioLegend (San Diego, CA). FITC-labeled anti-human CD11b Ab (clone: Bear1) and FITC-labeled anti-human CD62L Ab (clone: DREG56) were obtained from Beckman Coulter (Brea, CA). PE-labeled anti-human CD162 Ab (clone: TC2) was obtained from Novus Biologicals (Littleton, CO). DyLight488-labeled anti-mouse CD42c Ab was obtained from emfret ANALYTICS (Eibelstadt, Germany). Anti-human HRG monoclonal antibody (Rat) (#75–14) and anti-human HRG polyclonal antibody (Rabbit) were made in our laboratory.

2.2. Cell Preparation

In accordance with the ethics approval and guidelines of Okayama University, written informed consent was obtained from healthy volunteers (n = 5), and blood was drawn from the cubital vein. The blood was layered onto Polymorphprep (Axis-Shield, Oslo, Norway) prior to density-gradient centrifugation. The purified neutrophils were suspended in Hank's Balanced Salt Solution (HBSS) buffer. The EA.hy926 cells (ATCC CRL-2922), a hybridoma of Human Umbilical Vein Endothelial Cells (HUVEC) and human epithelial cell line A549, were cultured in Dulbecco's modified Eagle medium (ATCC) containing 10% fetal bovine serum (Life Technologies). These cells were grown in a humidified atmosphere and passaged every 3–4 days.

2.3. Purification of HRG from Human Plasma

HRG was purified from human plasma (supplied by the Japanese Red Cross Society) as previously described (Mori et al., 2003). In brief, human plasma was incubated with nickel–nitrilotriacetic acid (Ni-NTA) agarose (Qiagen, Hilden, Germany) for 2 h at 4 °C with gentle shaking. The gel was packed into a column and washed successively with 10 mM Tris-buffered saline (TBS) (pH 8.0) containing 10 mM imidazole and then 10 mM Tris-buffer (TB) (pH 8.0) containing 1 M NaCl. Human HRG was eluted by 0.5 M imidazole in 10 mM TBS (pH 8.0). The protein extract was further purified by a Mono Q column (GE Healthcare, Little Chalfont, UK) with NaCl gradient. Purified human HRG was identified by sodium dodecyl sulfate–polyacrylamide gel electrophoresis (SDS-PAGE) and Western blotting with a human HRG-specific antibody.

2.4. Cecal Ligation Puncture Model

All animal experiments were approved by the university's committee on animal experimentation and performed according to the guidelines of Okayama University on animal experiments. Male C57BL/6N mice (22–25 g, 7–8 wk) were obtained from Japan SLC (Shizuoka, Japan). Sepsis was induced in mice by CLP. Animals were anesthetized and a ligature was placed below the ileocecal valve. The cecum was punctured once (mild sepsis) or twice (severe sepsis) with an 18-gauge needle and then returned to the peritoneal cavity. Animals were treated with vehicle (phosphate-buffered saline (PBS)) or with 4 or 20 mg/kg of human HRG or protein control (human serum albumin (HSA); 20 mg/kg) immediately or 6 h and at 24 h and 48 h after CLP induction. Sham mice underwent the same surgical procedures without ligation and puncture.

2.5. Sickness Behavior

Sickness behaviors were evaluated at 24 h after CLP. Details of the assessments used and the scoring are as follows: 1 = normal (locomotion, appearance); 2 = slight signs of illness (lethargy, ptosis, or piloerection); 3 = obvious illness (very little movement, ptosis and piloerection, curled body posture); 4 = very sick animal (virtually no movement, impaired breathing, unresponsiveness, plus the above symptoms) (Sudom et al., 2004).

2.6. CLP Mice Model with the Imipenem-pretreatment

Sepsis was induced in mice by CLP. Animals were anesthetized and a ligature was placed below the ileocecal valve. The cecum was punctured twice with an 18-gauge needle and then returned to the peritoneal cavity. When the effects of imipenem were examined, imipenem was administered i.m. at 6 h or 12 h and HRG was administered at 12 h, 24 h, and 48 h after CLP induction.

2.7. Experiments with CLP Mice Samples

Whole blood from mouse heart at 24 h after CLP was plated on LB agar dishes and incubated at 37 °C; colony-forming units (CFUs) were counted after 24 h. The results were expressed as CFU/mL. The number of red blood cells (RBC), white blood cells (WBC), and platelet were counted in whole blood from mouse at 24 h after CLP (subcontract animal clinical examination: Oriental east, Tokyo, Japan). The blood was mixed with 3.2% sodium citrate solution (blood: sodium citrate solution = 9:1) and separated the plasma from the blood. The plasma samples were used for coagulation and fibrinolysis tests (subcontract animal clinical examination: Monoris, Tokyo, Japan) and albumin, aspartate transaminase (AST), and alanine transaminase (ALT) levels (subcontract animal clinical examination: Oriental east) (Table S2). The cells present in the peritoneal cavity were collected by injecting 5 mL of saline. The cells were counted using a Burker–Turk counting chamber.

2.8. Lung Wet-to-Dry Weight Ratio

The whole lung from mouse at 24 h after CLP treated with PBS, HSA, or HRG was weighed, dried in an oven at 65 °C for 48 h, and weighed again. The lung wet/dry weight ratio was then calculated.

2.9. Western Blot Analysis of HRG Levels in Plasma

Mouse plasma was electrophoresed on polyacrylamide gel (12.5%) and transferred onto a polyvinylidene diflouride (PVDF) membrane (Bio-Rad, Hercules, CA). After the membrane was stained with SYPRO Ruby (Life Technologies), it was blocked with 10% skim milk for 1 h and incubated overnight at 4 °C with rabbit anti-hHRG polyclonal Ab followed by anti-rabbit IgG goat polyclonal IgG-horseradish peroxidase (HRP) (MBL, Nagoya, Japan) for 2 h at room temperature (RT). The signals were finally visualized using an enhanced chemiluminescence system (Pierce Biotechnology, Rockford, IL).

2.10. In Vivo RNAi Experiments

Invivofectamine 2.0 reagent and HRG siRNA or negative control siRNA (Life Technologies) were mixed and incubated for 30 min at 50 °C. The mixtures were dialyzed by PBS and injected via tail veins of male C57BL/6 N mice (7 weeks old). Two, three, and seven days after injection, mouse blood was obtained by cutting the tail, and the plasma levels of HRG were determined using Western blotting. Then, a mild CLP sepsis (with one puncture) was induced in the RNAi-treated mice.

2.11. Ezyme-linked Immunosorbant Assay (ELISA)

In accordance with the ethics approval and guidelines of Okayama University, written informed consent was obtained from ten healthy subjects and eight septic patients. The septic patients were evaluated by clinical criteria of infections with SIRS according to 2001 guidelines (Levy et al., 2003). The plasma sample of septic patients was obtained on the first day of admission in intensive care unit. Human plasma HRG levels were assessed by ELISA using solid-phase-immobilized anti-HRG monoclonal antibodies (#75-14) and Ni-NTA labeled with HRP (Qiagen).

2.12. High-speed Scan Spinning-disk Confocal Microscopy System

Images were acquired with an inverted microscope IX 73 (Olympus, Tokyo, Japan) using a ×20/0.75 objective lens. The microscope was equipped with a CSU-X1 confocal scanner (Yokokawa, Tokyo, Japan) and an iXON3 EMCCD camera (Andor Technology, Belfast, Northern Ireland). Image acquisition software iQ2 (Andor Technology) was used to drive the confocal microscope.

2.13. In vivo Neutrophil Imaging

Neutrophils and platelets were stained with Alexa Fluor 594-labeled anti-Gr-1 antibody (10 μg/mouse) and DyLight488-labeled anti-CD42c antibody (2 μg/mouse), respectively, via i.v. injection before the *in vivo* imaging experiments. Sham-operated or CLP-treated mice were anesthetized with isoflurane, the abdomen was opened, and the exposed mesentery vessels were observed by a high-speed scan spinning-disk confocal microscopy system. Heating pads were used to keep the body temperature at 37 °C.

2.14. Micro Channel Array Flow Analyzer (MC-FAN)

The blood or neutrophil samples were prepared as follows. Mice were sacrificed 24 h after CLP. Blood was obtained from the heart and mixed with heparin for the hematocrit test or with acid–citrate–dextrose (ACD) solution for the microcapillary passage test. Human whole blood was withdrawn from the cubital vein and mixed with ACD solution. The blood was incubated with rat anti-human HRG monoclonal antibody (clone #75- 14) or rat IgG for 30 min at 37 °C. The human neutrophils isolated were treated with one of the reagents (bovine serum albumin (BSA), HSA, HRG, fMLP) for 1 h at 37 °C. The whole blood or neutrophil samples were forced to flow through artificial microchannels made of silicon (width 7 μm, depth 4.5 μm, length 30 μm) under a constant suction of −20 cm H_2O (Micro Channel Array Flow Analyzer; MC-FAN, MC Lab, Tokyo, Japan). The passage time of the 100 μl samples through microcapillaries was determined.

2.15. Immunohistochemistry

Immunohistochemical staining of nuclei, MPO, CD42d, and fibrinogen/fibrin was performed on 5 μm lung sections with DAPI, anti-mouse MPO Ab at 5 μg/ml followed by Alexa Fluor 488-labeled anti-goat IgG, anti-mouse CD42d Ab at 5 μg/ml followed by Alexa Fluor 568-labeled anti-sheep IgG, and anti-mouse fibrinogen/fibrin Ab at 5 μg/ml followed by Alexa Fluor 647-labeled anti-rabbit IgG after antigen retrieval; incubation of the lung section with Target Retrieval Solution, pH 9 (DAKO, Glostrup, Denmark) for 10 min at 120 °C. In other set of experiments, the nuclei, MPO, and cit-histone H3 were stained on 5 μm lung sections with SYTOX Green, anti-mouse MPO Ab at 5 μg/ml followed by Alexa Fluor 568-labeled anti-goat IgG and anti-cit-histone H3 Ab at 5 μg/ml followed by Alexa Fluor 405-labeled anti-rabbit IgG after antigen retrieval; incubation of the lung section with Target Retrieval Solution, pH 9 (DAKO) for 10 min at 120 °C. Immunohistochemical staining of nuclei, MPO, HRG, and fibrinogen/fibrin was performed on 5 μm lung sections with DAPI, anti-mouse MPO Ab at 5 μg/ml followed by Alexa Fluor 488-labeled anti-goat IgG, anti-HRG Ab at 5 μg/ml followed by Alexa Fluor 568-labeled anti-rabbit IgG, and anti-mouse fibrinogen/fibrin Ab at 5 μg/ml followed by Alexa Fluor 647-labeled anti-sheep IgG after antigen retrieval; incubation of the lung section with Target Retrieval Solution, pH 6.1 (DAKO) for 10 min at 120 °C. Immunohistochemical staining of nuclei and Gr-1 was performed on 5 μm lung sections with SYTOX Blue and Alexa Fluor 594-labeled rat anti-mouse Gr-1 Ab at 5 μg/ml after antigen retrieval; incubation of the lung section with 0.3% pepsin (Sigma) for 30 min at 37 °C. MPO-positive neutrophils and neutrophil extracellular traps (NETs) (cit-histone H3 positive site) were counted in three fields of a lung section at ×200 magnification under a confocal laser scanning microscopy. The number of MPO, CD42d, and fibrin/fibrinogen triple positive sites was counted in three fields of a lung section at ×400 magnification under a confocal laser scanning microscopy. The results were expressed as the number of MPO-positive neutrophils, MPO, CD42d, and fibrin/fibrinogen triple positive sites and NETs per square millimeter. The number of CD42d- and fibrin/fibrinogen-positive sites among MPO-positive neutrophils in each group were also determined.

2.16. Primer Sequence for Real-time Polymerase Chain Reaction (PCR)

Glyceraldehyde-3-phosphate dehydrogenase (GAPDH) (NM_008084) F-5′ TGA CGT GCC GCC TGG AGA AA 3′, R-5′ AGT GTA GCC CAA GAT GCC CTT CAG 3′; tumor necrosis factor (TNF)-α (NM_013693) F-5′ GAC CCT CAC ACT CAG ATC ATC CTT CT 3′, R-5′ GCG CTG GCT CAG CCA CTC 3′; inducible nitric oxide synthase (iNOS) (NM_010927) F-5′ GAT TTT GCA TGA CAC TCT TCA 3′, R-5′ GGA GCC ATA ATA CTG GTT GAT 3′; IL-6 (NM_031168) F-5′ GAC CTG TCT ATA CCA CTT CAC A 3′, R-5′ CTC TGG AAG TTT CAG ATT GTT 3′; plasminogen activator inhibitor-1 (PAI-1) (NM_008871) F-5′ CTA TGG CGT GTC CTC GGT GCT 3′, R-5′ CAT TCT TGT TCC ACG GCC CCA T 3′; neutrophil elastase (NM_015779) F-5′ CTA CTG GCA TTG TTC CTG GGT G 3′, R-5′ GCT GAC ATG ACG AAG TTC CTG G 3′; receptor for advanced glycation end products (RAGE) (NM_007425) F-5'CTA GAG CCT GGG TGC TGG TTC 3′; R-5′ GTT TCC ATT CTA GCT GCT GGG GC 3′; HRG (NM_053176) F-5′ TGC TCA CCA CAG CAT TGC TT 3′; R-5′ CAC TCC TCC GCC CTT TAT TGA 3′.

2.17. Real-time Quantitative PCR

Total RNA was isolated from the mouse lung or liver using an RNeasy mini kit (Qiagen). Complementary DNA was synthesized with a Takara RNA PCR kit Ver. 3.0 (Takara Bio, Nagahama, Japan) according to the manufacturer's instructions. Real-time PCR was performed with a Light Cycler (Roche, Basel, Switzerland) according to the manufacturer's instructions. Reaction mixtures contained cDNA template, SYBR premix Ex Taq (Takara Bio), and sequence-specific primers. GAPDH expression was used to normalize cDNA levels. The PCR products were analyzed by a melting curve to ascertain the specificity of amplification.

2.18. HRG Digestion Assay

HSA (4 μg) or HRG (4 μg) was mixed with or without thrombin (30 U/ml) and incubated for 4 h at 37 °C. The reaction mixtures were analyzed by SDS-PAGE with Coomassie brilliant blue staining.

2.19. Cytometric Bead Array (CBA)

IL-6, TNF-α, and IL-10 concentration in the serum from mouse at 24 h after CLP treated with PBS, HSA, and HRG were measured by CBA kits according to the manufacturer's instructions (BD Biosciences, Franklin Lakes, NJ).

2.20. Neutrophil Shape and Adhesion Assay

Purified human neutrophils pre-stained with Hoechst33342 (Nuclei) and Calcein-AM (Cytosol) were aliquoted in a volume of 100 μl (5×10^4 cells/well) to polystyrene wells or confluent wells of EA.hy926 cells (ATCC CRL-2922), a hybridoma of HUVEC and the human epithelial cell line A549. The incubation started with one of the reagents (BSA, HSA, HRG, fMLP: each at a final concentration 1 μM) and continued for indicated periods at 37 °C. The cell shape and fluorescence intensity were analyzed by using an In Cell Analyzer 2000 (GE Healthcare) and In Cell Analyzer Workstation software (GE Healthcare). Neutrophil adhesion was evaluated by measuring the fluorescence intensity of the wells by a Flexstation 3 (Molecular Devices, Sunnyvale, CA) before and after the wells were gently washed twice to remove any nonadherent cells. When HRG's effects on intracellular calcium were examined, BAPTA or Fluo-4-AM was preloaded for 20 min.

2.21. F-actin Distribution and Cell Surface Structure in Neutrophils

Neutrophils (5×10^6 cells/ml) were seeded onto poly L-lysine-coated cover glass (Matsunami, Tokyo, Japan) and incubated with one of the reagents (BSA, HSA, HRG, or fMLP: each at a final concentration of 1 μM) at 37 °C for 1 h. For actin staining, the neutrophils were fixed with 4% PFA and treated with 0.1% TritonX-100 followed by staining with Phalloidin-Alexa568 (F-actin), DNaseI-Alexa488 (G-actin), and DAPI (Nuclei). The samples were observed using a confocal microscope (LSM 510, Carl Zeiss, Oberkochen, Germany). For electron microscopy, the samples were fixed in 4% paraformaldehyde and 2.5% glutaraldehyde for 24 h at 4 °C, then post-fixed using 1% osmium tetroxide for 1 h at 4 °C. OsO_4 coating with an osmium coater HPC-1S (Vacuum Device, Mito, Japan) was used. Each sample was examined using an s-4800 scanning laser microscope (Hitachi, Tokyo, Japan).

2.22. Determination of ROS Production

The neutrophil suspension with isoluminol (final concentration, 50 μM) and horse radish peroxidase type IV (final concentration 4 U/ml) were aliquoted to a 96-well plate (BD Biosciences) in a volume of 100 μl (5×10^4 cells) with one of the reagents (BSA, HSA, HRG, each at a final concentration of 1 μM). Neutrophil extracellular ROS production was evaluated at 15 min after the start of incubation at 37 °C by the measurement of chemiluminescence intensity using Flexstation 3. Intracellular ROS was determined by pre-loading of CM-H2DCFDA into neutrophils for 20 min.

2.23. Detection of Intercellular Adhesion Molecule-1 (ICAM-1), P-selectin and Phosphatidylserine on EA.hy926 Cell

EA.hy926 cell monolayer was gently washed twice by PBS to remove culture medium and was stimulated by the mixture of HBSS, BSA, HSA or HRG (1 μM each), and LPS (10 ng/ml) or TNF-α (10 ng/ml) for 30 min at 37 °C in 5% CO_2 atmosphere. The cells were fixed by 10% formalin after PBS washing twice and were incubated with 0.1% Triton-X100 TBS buffer for 10 min. These fixed cells were stained by Alexa Fluor 488-labeled anti-human CD54 Ab or DyLight 488-labeled anti-human CD62P Ab for 2 h at RT, or anti-phosphatidylserine Ab followed by Alexa Fluor 488-labeled anti-rabbit IgG for 1 h at RT. The number of phosphatidylserine-positive cells was counted in six fields at ×100 magnification under a confocal laser scanning microscopy. The number of CD54- or CD62P-positive cells was counted in four fields at ×200 magnification under a confocal laser scanning microscopy.

2.24. Chemotaxis Assay

The transfer of neutrophils to the vertical direction was examined using a 24-well Chemotaxicell chamber (Kurabo, Kurashiki, Japan). Neutrophils (5×10^5 cells in 100 μl) were added to the upper wells of the chamber and were separated by a polycarbonate membrane 5 μm in diameter pores from lower wells containing one of the reagents (BSA, HSA, HRG, or fMLP). Following 1 h incubation, the cells that had migrated to lower wells were counted under a light microscope. For the horizontal chemotaxis assay, neutrophils (5×10^5 cells/ 10 μl) with or without HRG (1 μM) were added to one well in agarose gel (5 mm thick) and were allowed to migrate toward the other well (2 mm from the former) containing a possible chemoattractant (1 μM). Two hours after the start of migration, the neutrophils were fixed and stained with Wright's stain, and the distance from the origin to the leading edge was measured.

2.25. FACS Analysis

C5a, IL-8, or fMLP was preincubated with HSA or HRG for 1 h at 37 °C. Purified human neutrophils were stimulated with the mixture for 1 h at 37 °C in 5% CO_2 atmosphere. The stimulation was stopped by ice-cold cooling for 10 min. The neutrophils were stained by FITC-labeled anti-human CD11b Ab, FITC-labeled anti-human-activated CD11b Ab, FITC-labeled anti-human CD62L Ab, or PE-labeled anti-human CD162 Ab for 25 min at 4 °C. The fluorescence intensity of the cells was detected

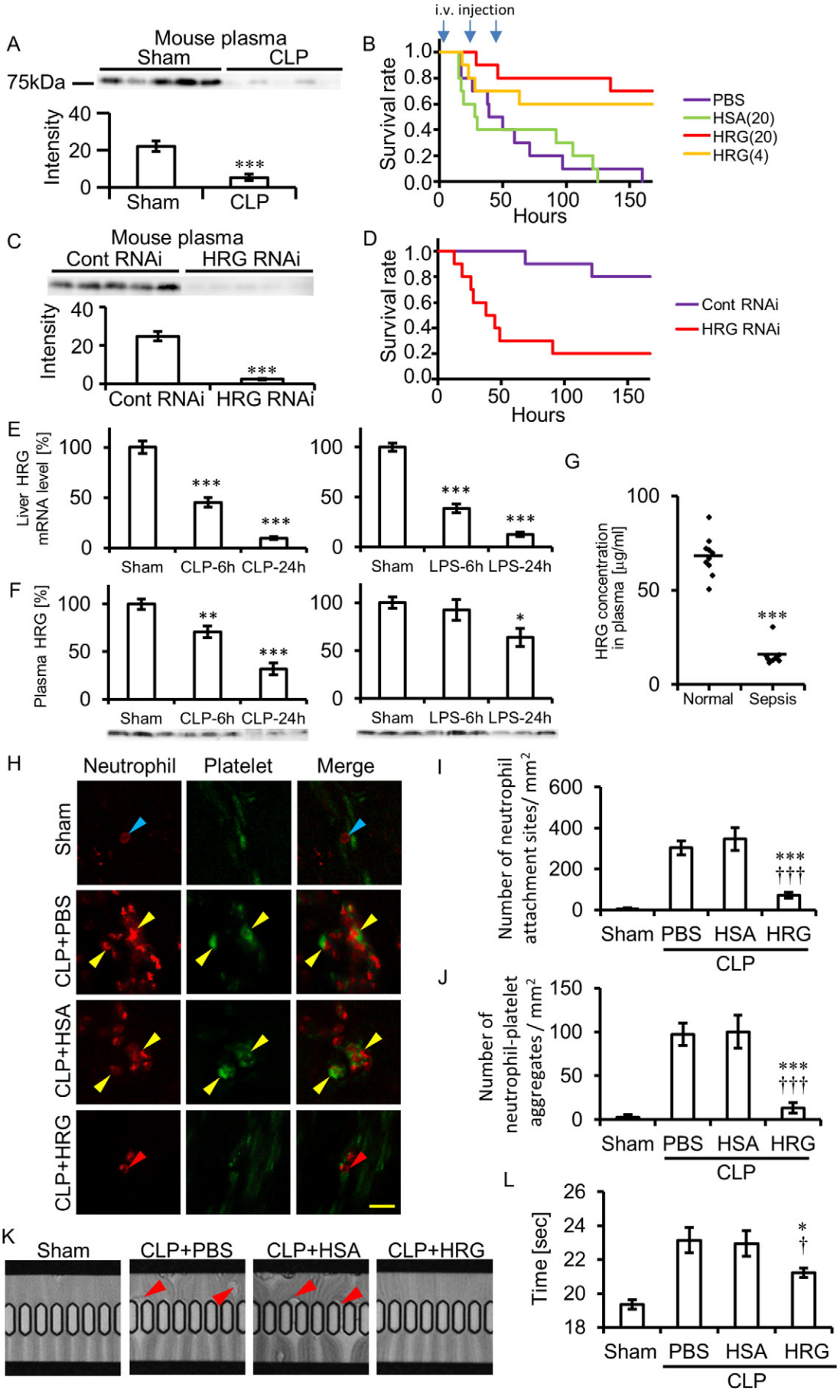
A
Mouse plasma
Sham
CLP
75kDa
Intensity
40
20
0
***
Sham
CLP
B
i.v. injection
Survival rate
1.0
0.8
0.6
0.4
0.2
0.0
0
50
100
150
Hours
PBS
HSA(20)
HRG(20)
HRG(4)
C
Mouse plasma
Cont RNAi
HRG RNAi
Intensity
40
20
0
***
Cont RNAi
HRG RNAi
D
Survival rate
1.0
0.8
0.6
0.4
0.2
0.0
0
50
100
150
Hours
Cont RNAi
HRG RNAi
E
Liver HRG mRNA level [%]
100
50
0
***
***
Sham
CLP-6h
CLP-24h
100
50
0
***
***
Sham
LPS-6h
LPS-24h
F
Plasma HRG [%]
100
50
0
**
***
Sham
CLP-6h
CLP-24h
100
50
0
*
Sham
LPS-6h
LPS-24h
G
HRG concentration in plasma [μg/ml]
100
50
0
***
Normal
Sepsis
H
Neutrophil
Platelet
Merge
Sham
CLP+PBS
CLP+HSA
CLP+HRG
I
Number of neutrophil attachment sites/ mm²
600
400
200
0
***
†††
Sham
PBS
HSA
HRG
CLP
J
Number of neutrophil-platelet aggregates / mm²
150
100
50
0
***
†††
Sham
PBS
HSA
HRG
CLP
K
Sham
CLP+PBS
CLP+HSA
CLP+HRG
L
Time [sec]
26
24
22
20
18
*
†
Sham
PBS
HSA
HRG
CLP

by FACS calibur (BD Biosciences). These data were analyzed by Flow Jo software (TOMY Digital Biology, Tokyo, Japan).

2.26. Statistical Analysis

The statistical analysis across multiple treatment groups was determined with ANOVA, followed by Dunnett test. The statistical difference between paired groups were determined using Mann–Whitney test. All data are presented as the means ± standard error (SEM). P values <0.05 were considered statistically significant. The Kaplan–Meier method was used for the survival experiments, and the differences were analyzed using the log-rank test.

3. Results

3.1. Effects of HRG on Lethality of CLP Septic Mice

In CLP, a mouse model of sepsis, plasma HRG levels decreased significantly, by 77%, compared with the sham control levels 24 h after CLP (Fig. 1A). The survival rate of mice treated with PBS for 3 days after CLP was 0% at day 7. The administration of purified human HRG (4 and 20 mg/kg, i.v.) for 3 days significantly improved lethality in CLP mice, whereas the same dose of HSA (20 mg/kg, i.v.) had no effect on the survival rate, indicating the clear survival effects of i.v. injection of HRG (Fig. 1B). In addition to survival rate, locomotor activity of mice treated with HRG was improved clearly (Fig. S1A). The therapeutic time window of i.v. HRG appeared to be 6 h of the CLP induction in which only 30% survival rate was obtained (Fig. S1B). However, when imipenem (25 mg/kg) was administered i.m. 6 h or 12 h after CLP, the therapeutic time window of i.v. HRG was prolonged to 12 h after CLP (Figs. S1C and S1D). The CFU of the blood from three groups of mice treated with PBS, HSA, and HRG showed similar values (Fig. S1E). Also, the total number of infiltrating cells in the peritoneal cavity did not differ among the groups (Fig. S1F). These results suggested that the beneficial effects of HRG were not ascribable to the increase in bacteriocidal activity (Shannon et al., 2010) in the peritoneal cavity.

Pretreatment of mice with siRNA for mouse HRG reduced plasma levels of HRG by 90% at 5 days after i.v. injection as compared with those in nonrelevant siRNA-treated mice (Fig. 1C). The half-life of HRG in mouse blood was estimated to be 15 h after siRNA injection, based on the decline curve of plasma HRG (Fig. S1G). The survival rate of HRG-knockdown mice after mild CLP (one cecum penetration by needle) was compared with that in control mice to see whether the depletion of HRG from plasma could exacerbate septic inflammation and lethality. The results clearly indicated that depletion of HRG reduced the survival rate significantly (Fig. 1D). HRG mRNA levels decreased time-dependently after CLP or LPS injection, leading to less than 15% of sham control at 24 h (Fig. 1E). The resultant plasma levels of HRG in CLP mice were less than that in LPS-injected mice (Fig. 1F). Moreover, plasma HRG levels in septic patients decreased significantly, by 77%, compared with those in healthy volunteers (Fig. 1G; Table S1), indicating a similar dynamics of plasma HRG in septic patients to those in septic mice. Taken together, the results of our experiments on supplementary treatment with HRG and the acute depletion of HRG strongly suggested that HRG may be an important plasma factor controlling the lethality of mice in septic conditions.

3.2. Effects of HRG on Microcapillary Passage of Blood in CLP Mice

In vivo imaging of circulating neutrophils labeled with anti-Gr-1 Ab and platelets labeled with anti-CD42c Ab showed that the spherical shape of neutrophils and platelets circulated with different velocities in both mesenteric arterioles and venules in sham-operated mice. Rolling, spherical neutrophils on the VECs were sometimes observed along the marginal flow of the blood-stream in venules in sham mice (Fig. 1H; Movie S1). Transient oval or teardrop shape changes were observed in the arterioles of sham mice. In contrast, deformed neutrophils with a multiangular and rigid appearance were observed in the circulation in CLP mice. Extremely deformed neutrophils were attached to VECs in venules and were arrested there without migration during the observation periods (Fig. 1I; Movie S1). Moreover, the accumulation of platelets occurred on those deformed neutrophils (Fig. 1J; Movie S1). Thus, the extreme morphological changes of circulating neutrophils and the enhanced interaction with VECs demonstrated by *in vivo* imaging appear to represent pathological features in the septic mouse model. In contrast, HRG-treated mice showed the spherical neutrophils in the circulation and had markedly fewer neutrophils and aggregated platelets attached to endothelial cells in venules compared with control CLP mice (Fig. 1H–J; Movie S1), strongly suggesting the less interaction of circulating neutrophils with VECs in these mice.

The microcapillary passage of peripheral blood from CLP mice was examined using a MC-FAN *ex vivo* (Fig. 1K; Movie S2). In mice treated with PBS or HSA, deformed leukocytes were attached to the microcapillary entrance very often indicated by red arrowheads, whereas there were few such leukocytes in HRG-treated mice (Fig. 1 K; Movie S2). The time required for the passage of 100 μl blood through the microcapillary reflected the adhesion of leukocytes (Fig. 1L). On the other hand, there were no significant differences in hematocrit levels among the treated groups (Fig. S1H).

3.3. Analysis of HRG Effects on Septic ARDS

Hematoxylin–eosin staining of lung tissue revealed lung inflammation 24 h after CLP in mice treated with PBS and HSA; this inflammation included increased thickness of the interstitial space of alveoli, infiltration of neutrophils, and congestion/hemorrhage (Fig. 2A). However, HRG treatment (20 mg/kg, i.v.) ameliorated pathological findings in the lung remarkably (Fig. 2A). Measurement of wet/dry weight ratio showed that HRG treatment inhibited lung edema significantly (Fig. 2B). Also, the number of neutrophils in the lung detected by anti-MPO Ab increased significantly in CLP mice treated with PBS and HSA, and HRG treatment inhibited the number of neutrophils by 55% (Fig. 2C

Fig. 1. *HRG's effects on the mortality of CLP mice and the passage of neutrophils through microcapillaries.* (*A*) CLP was performed in mice, and plasma levels of HRG were determined 24 h after CLP by Western blotting. Quantification of the results of Western blotting. $^{***}P<0.001$ *vs.* sham. (*B*) Kaplan–Meier survival curve of mice with CLP. PBS, HSA (20 mg/kg), or human-purified HRG (4 or 20 mg/kg) was administered i.v. 10 min, 24 h, and 48 h after CLP. (*C*) Effects of knockdown of liver HRG by siRNA on the plasma levels of HRG. The plasma levels were determined immediately before CLP by Western blotting. Quantification of the results of Western blotting. $^{***}P<0.001$ *vs.* Control RNAi. (*D*) Effects of knockdown of liver HRG by siRNA on the survival of mild-CLP mice. (*E*) Determination of HRG mRNAs in the liver of CLP or LPS (10 mg/kg i.v.) -injected mice. The tissue samples for real-time PCR were collected 6 or 24 h after CLP or LPS injection. The relative expression levels of HRG mRNA in the liver were calculated as % of sham control. $^{***}P<0.001$ *vs.* sham. (*F*) Plasma levels of HRG were determined 6 or 24 h after CLP or LPS injection by Western blotting. The relative expression levels were calculated as % of sham control. $^{*}P<0.05$, $^{**}P<0.01$, and $^{***}P<0.001$ *vs.* sham. (*G*) Decreased plasma HRG levels in human sepsis. HRG levels were determined by ELISA. Individual symbols represent individual donors and horizontal lines indicate mean. $^{***}P<0.001$ *vs.* normal. (*H*) *In vivo* imaging of circulating neutrophils and platelets in CLP mice. The neutrophils (red) and platelets (green) were labeled by i.v. injection of anti-Gr-1 and anti-CD42c antibodies 12 h after CLP, and the circulating neutrophils and platelets were observed under an *in vivo* imaging system. Blue arrowheads indicate the circulating neutrophil. Red arrowheads indicate the neutrophil attached to the vascular wall. Yellow arrowhead indicates the sites where neutrophils and platelets were attached to the vascular wall together (see Movie S1). Scale bar, 20 μm. (*I*) The attachment sites of neutrophils or (*J*) neutrophils-platelets clots attached to the mesentery vessel wall were counted in each group. $^{***}P<0.001$ and $^{\dagger\dagger\dagger}P<0.001$ *vs.* PBS and HSA, respectively. (*K*) Whole blood of CLP mice was withdrawn 24 h after CLP and applied to a MC-FAN. The red arrowheads indicate the leukocytes attached to the tops of microcapillaries. (*L*) The time required for the passage of 100 μl of whole blood was determined using a MC-FAN in four groups. $^{*}P<0.05$ and $^{\dagger}P<0.05$ *vs.* PBS and HSA, respectively. The results shown are the means ± SEM of five mice (*A*, *C*, *E*, *F*, *I*, *J*, and *L*) or ten healthy volunteers and eight septic patients (*G*). Ten mice were used in each group (*B* and *D*).

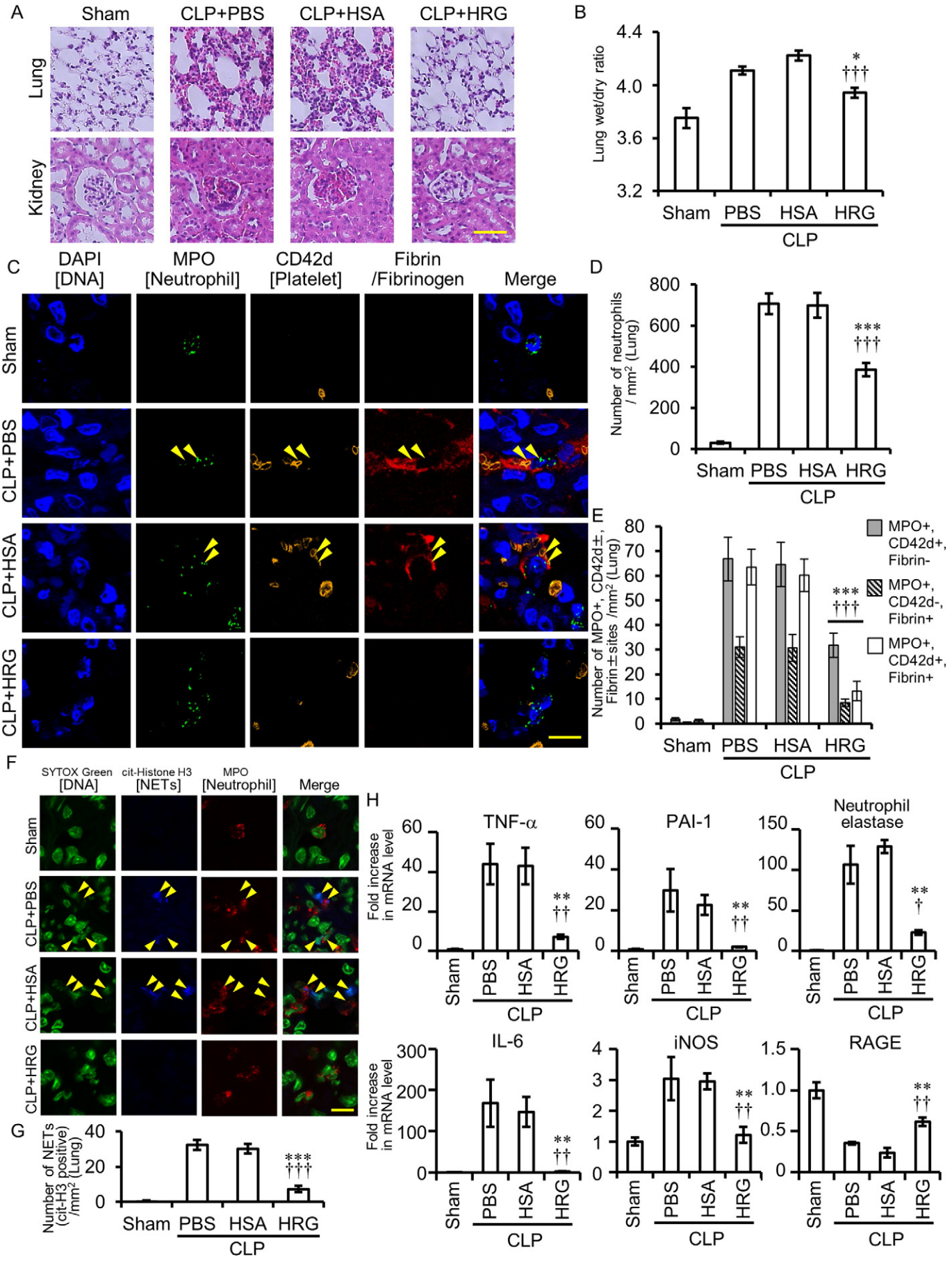
A
Sham
CLP+PBS
CLP+HSA
CLP+HRG
Lung
Kidney
B
Lung wet/dry ratio
4.4
4.0
3.6
3.2
*
†††
Sham PBS HSA HRG
CLP
C
DAPI [DNA]
MPO [Neutrophil]
CD42d [Platelet]
Fibrin /Fibrinogen
Merge
Sham
CLP+PBS
CLP+HSA
CLP+HRG
D
Number of neutrophils / mm² (Lung)
800
600
400
200
0
***
†††
Sham PBS HSA HRG
CLP
E
Number of MPO+, CD42d±, Fibrin±sites /mm² (Lung)
80
70
60
50
40
30
20
10
0
***
†††
MPO+, CD42d+, Fibrin-
MPO+, CD42d-, Fibrin+
MPO+, CD42d+, Fibrin+
Sham PBS HSA HRG
CLP
F
SYTOX Green [DNA]
cit-Histone H3 [NETs]
MPO [Neutrophil]
Merge
Sham
CLP+PBS
CLP+HSA
CLP+HRG
G
Number of NETs (cit-H3 positive) /mm² (Lung)
40
20
0
***
†††
Sham PBS HSA HRG
CLP
H
Fold increase in mRNA level
TNF-α
PAI-1
Neutrophil elastase
IL-6
iNOS
RAGE
Sham PBS HSA HRG
CLP

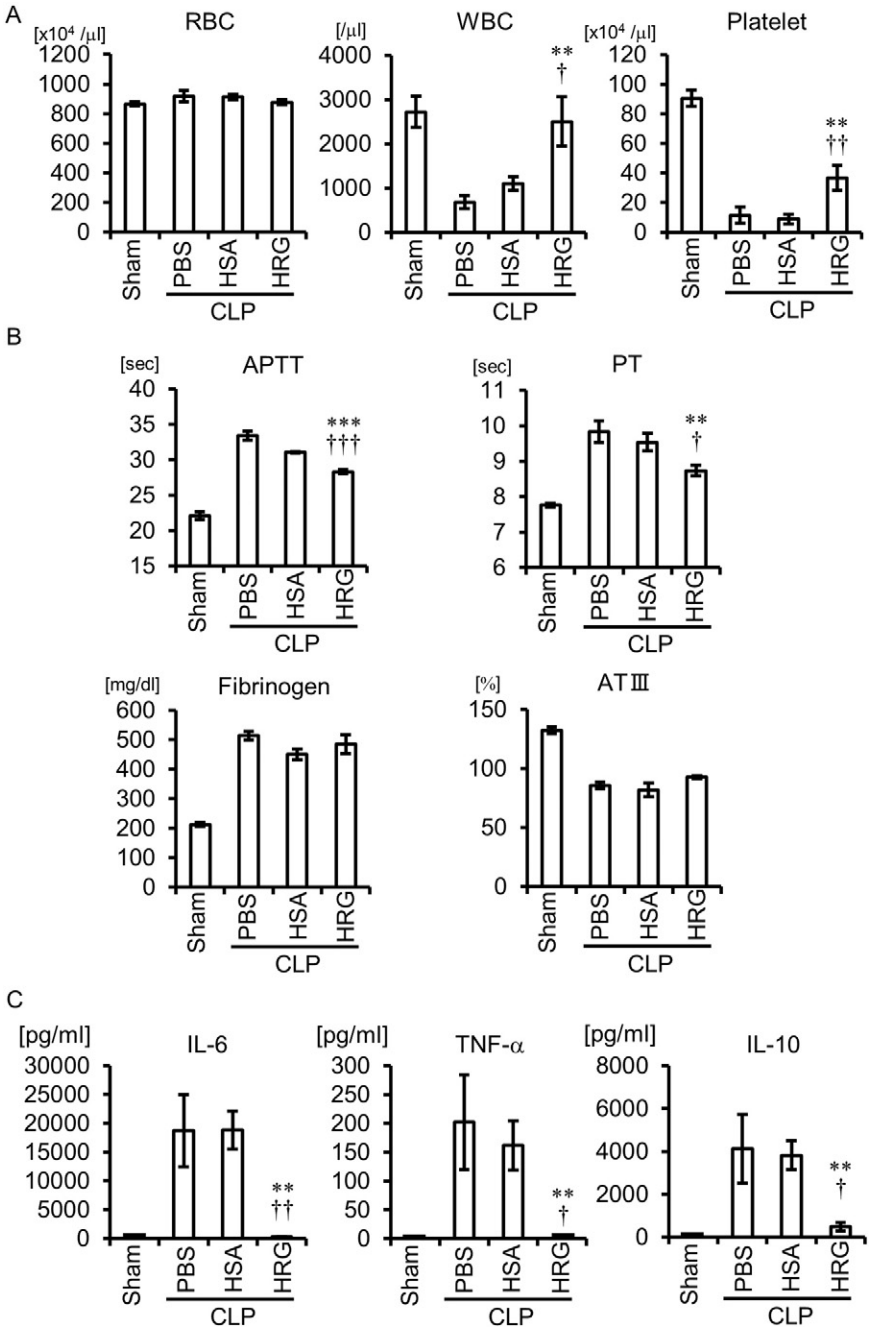

Fig. 3. *Effects of HRG treatment on the number of blood cells, coagulation, and hypercytokinemia in CLP mice.* (*A*) The whole blood samples were collected 24 h after CLP. The results shown are the means ± SEM of five mice. $^{**}P < 0.01$ *vs.* PBS. $^{\dagger}P < 0.05$ and $^{\dagger\dagger}P < 0.01$ *vs.* HSA. (*B*) The plasma samples for coagulation test were collected 24 h after CLP. The results shown are the means ± SEM of six mice. $^{**}P < 0.01$, $^{***}P < 0.001$ *vs.* PBS. $^{\dagger}P < 0.05$ and $^{\dagger\dagger\dagger}P < 0.001$ *vs.* HSA. (*C*) The serum samples for the determination of cytokines were collected 24 h after CLP. The results shown are the means ± SEM of five mice. $^{**}P < 0.01$ *vs.* PBS. $^{\dagger}P < 0.05$ and $^{\dagger\dagger}P < 0.01$ *vs.* HSA.

Fig. 2. *Effects of HRG treatment on inflammation in lungs and kidneys of CLP mice.* (*A*) CLP mice treated with PBS, HSA, or HRG were fixed at 24 h after CLP. Paraffin-embedded sections of the lungs (upper) and kidneys (lower) were stained with HE. (*B*) Edema of the lung was evaluated in each group as a ratio of wet to dry lung tissue weight. $^{*}P < 0.05$, $^{\dagger\dagger\dagger}P < 0.001$ *vs.* PBS and HSA, respectively. (*C*) The lungs of CLP mice were stained by DAPI (nuclei: blue), anti-MPO antibody (neutrophil: green), anti-CD42d antibody (platelet: orange), and anti-fibrinogen/fibrin antibody (fibrin: red) followed by fluorescence detection. Yellow arrowheads indicate MPO, CD42d, and fibrin triple-positive sites. (*D*) Neutrophils in the lungs were counted in each group. $^{***}P < 0.001$, $^{\dagger\dagger\dagger}P < 0.001$ *vs.* PBS and HSA, respectively. (*E*) The number of MPO-positive, CD42d-postive or negative, and fibrin-positive or negative sites in the lungs was counted in each group. $^{***}P < 0.001$, $^{\dagger\dagger\dagger}P < 0.001$ *vs.* PBS and HSA, respectively. (*F*) The lungs of CLP mice were stained by SYTOX Green (nuclei: green), anti-MPO antibody (neutrophil: red) and anti-cit-histone H3 antibody (NET: blue) followed by fluorescence detection. Yellow arrowheads indicate NETs. (*G*) NETs (cit-histone H3 positive sites) in the lungs were counted in each group. $^{***}P < 0.001$, $^{\dagger\dagger\dagger}P < 0.001$ *vs.* PBS and HSA, respectively. (*H*) Determination of mRNAs of TNF-α, IL-6, PAI-1, iNOS, neutrophil elastase, and RAGE in lungs of CLP mice. The tissue samples for real-time PCR were collected 24 h after CLP. The relative expression levels were calculated treating sham control as one unit. $^{**}P < 0.01$ *vs.* PBS. $^{\dagger}P < 0.05$ and $^{\dagger\dagger}P < 0.01$ *vs.* HSA. The results shown are the means ± SEM of five mice (*B*, *D*, *E*, *G*, and *H*). Scale bars, 50 μm (*A*). Scale bars, 10 μm (*C* and *F*).

and D). Triple immunohistochemical staining of neutrophil, platelet and fibrin clearly revealed the existence of immunothrombi composed of neutrophil adhesion to vascular wall, platelet aggregation, and fibrin deposits in CLP mice treated with PBS or HSA (Fig. 2C and E), whereas the total number of overlapping spots in mice treated with HRG was much lower (Fig. 2C and E). HRG inhibited the deposition of fibrin on neutrophils and platelets (Fig. 2E). HRG immunoreactivities were observed on neutrophils from sham and CLP mice (on immunothrombus) (Fig. S2A). Extracellular localization of DNA associated with citrullinated histone H3 specific for NETosis (yellow arrowheads) was evident on

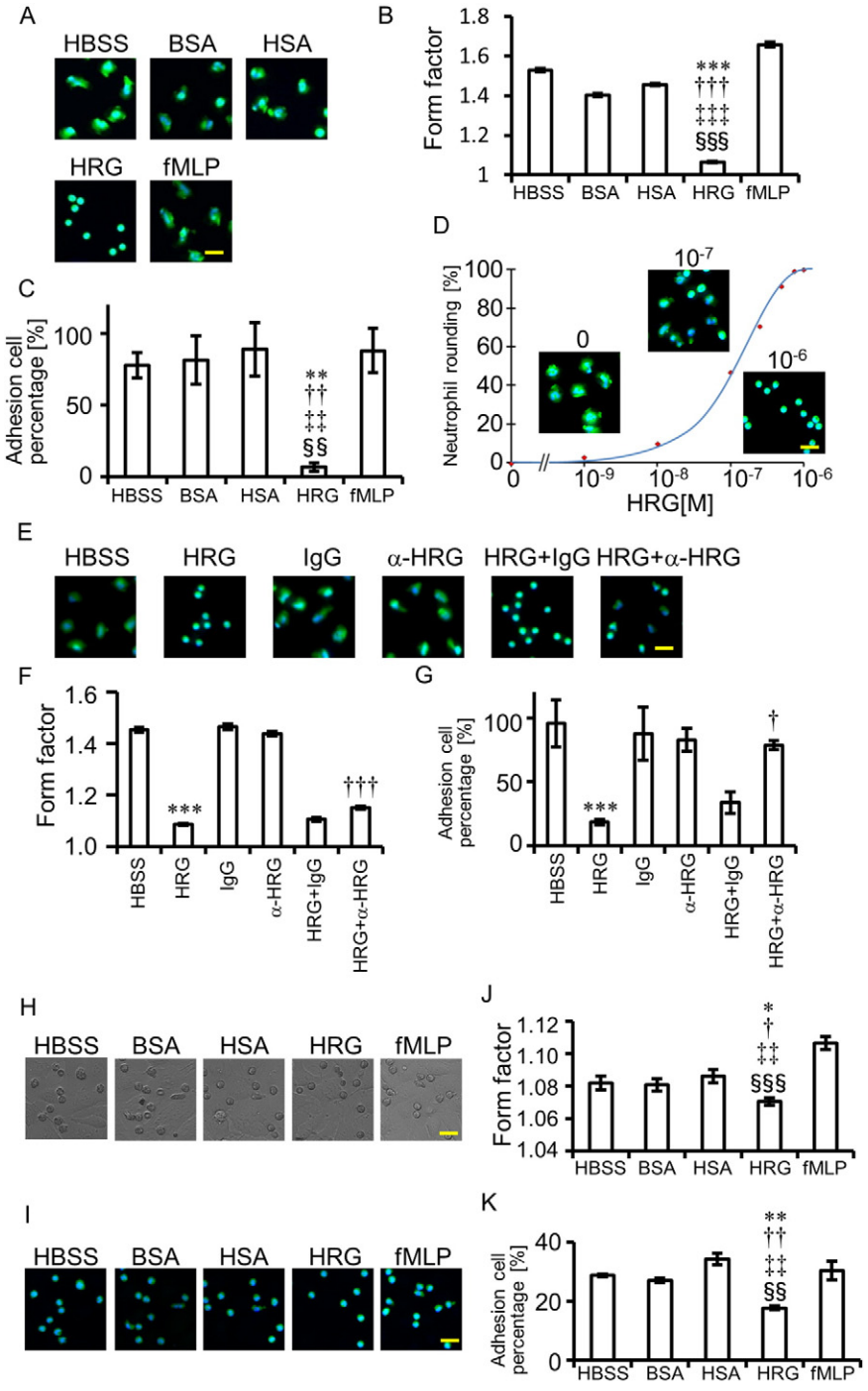

Fig. 4. *HRG's spherical-shape-inducing and adhesion-increasing effects on purified human neutrophils.* (*A*, *H*, and *I*) Purified human neutrophils were labeled with calcein-AM (green) and Hoechst33342 (blue) for 20 min. The neutrophils were incubated with reagents (1 μM) on polystyrene surface (*A*) or a monolayer of EA.hy926 (*H* and *I*) for 60 min and the neutrophil shape was observed under a fluorescent microscope (*A* and *I*) or a differential interference contrast microscope (*H*). (*B* and *J*). The rounding of neutrophils was analyzed by the In Cell Analyzer. Form factor (max diameter/ min diameter) was determined. One unit represents an ideal spherical shape. $^{*}P < 0.05$, $^{***}P < 0.001$ *vs.* HBSS. $^{\dagger}P < 0.05$, $^{\dagger\dagger\dagger}P < 0.001$ *vs.* BSA. $^{\ddagger\ddagger}P < 0.01$, $^{\ddagger\ddagger\ddagger}P < 0.001$ *vs.* HSA. $^{\S\S\S}P < 0.001$ *vs.* fMLP. (*C* and *K*) After gentle washing of the microtiter plate with HBSS twice, the residual cell numbers were counted and expressed as percentages of the initial cell numbers. $^{**}P < 0.01$, $^{\dagger\dagger}P < 0.01$, $^{\ddagger\ddagger}P < 0.01$, and $^{\S\S}P < 0.01$ *vs.* HBSS, BSA, HSA, and fMLP, respectively. (*D*) The concentration-effect curve was drawn by the plot of a spherical shape at different concentrations of HRG. The maximal roundness at 1 μM of HRG was expressed as 100%. (*E*) Effects of polyclonal antibody against HRG on HRG-induced induction of spherical shape in neutrophils. Anti-HRG Ab (300 μg/ml) or control IgG was added simultaneously with HRG and the incubation continued for 1 h. (*F*) Quantitative analysis of the effects of specific antibodies against HRG on neutrophil shape. $^{***}P < 0.001$ and $^{\dagger\dagger\dagger}P < 0.001$ *vs.* HBSS and HRG + IgG groups, respectively. (*G*) Effects of specific antibody against HRG on adhesion of neutrophils. $^{***}P < 0.001$ and $^{\dagger}P < 0.05$ *vs.* HBSS and HRG + IgG, respectively. The results shown are the means ± SEM of three experiments (*B*, *C*, *D*, *F*, *G*, *J*, and *K*). Scale bars, 20 μm.

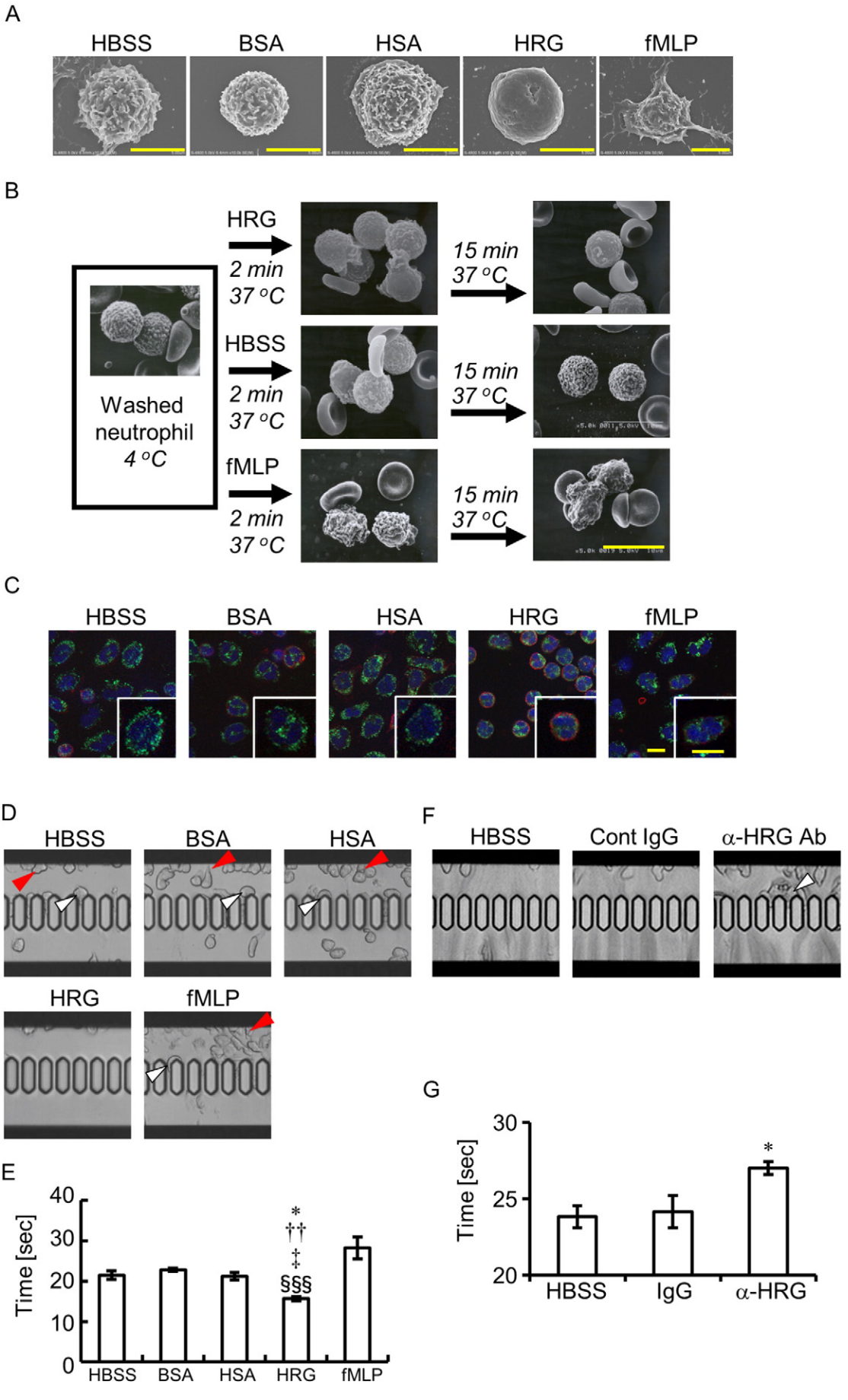
A
HBSS
BSA
HSA
HRG
fMLP
B
Washed neutrophil 4 °C
HRG
2 min 37 °C
HBSS
2 min 37 °C
fMLP
2 min 37 °C
15 min 37 °C
15 min 37 °C
15 min 37 °C
C
HBSS
BSA
HSA
HRG
fMLP
D
HBSS
BSA
HSA
HRG
fMLP
F
HBSS
Cont IgG
α-HRG Ab
E
Time [sec]
40
30
20
10
0
HBSS
BSA
HSA
HRG
fMLP
*
††
‡
§§§
G
Time [sec]
30
25
20
HBSS
IgG
α-HRG
*

immunothrombosis (Figs. 2F and S3). The NETs in CLP mice treated with PBS or HSA were significantly higher than that in sham mice and the treatment with HRG inhibited the number of NETs (Fig. 2G). In consistency with these histological findings, the results of mRNA expression of TNF-α, IL-6, PAI-1, iNOS, and neutrophil elastase in the lung using real-time PCR at 24 h clearly showed the significant upregulation of these mRNAs in CLP mice treated with PBS or HSA, whereas HRG treatment strongly suppressed the mRNAs of all of these, especially in the cases of IL-6 and PAI-1 (a marker of VEC damage) (Fig. 2H). Thus, it is likely that HRG suppressed the inflammatory responses in septic ARDS efficiently. The expression of RAGE mRNA in the lung was inversely regulated by CLP and HRG. HRG treatment inhibited glomerular leukocyte infiltration, increase in mesangeal matrix and renal tubular swelling in CLP mice observed at 24 h (Fig. 2A).

3.4. Effects of HRG on Coagulation and Hypercytokinemia in CLP Septic Mice

The platelet counts in CLP mice treated with PBS or HSA were significantly lower than that in sham mice, and the treatment with HRG restored the platelet counts (Fig. 3A). Consistent with the consumption of platelets in CLP mice treated with PBS or HSA, disorder markers of intrinsic and extrinsic coagulation pathways, such as activated partial thromboplastin time (APTT) and prothrombin time (PT) values, were prolonged in these mice compared with sham control value (Fig. 3B). HRG treatment significantly reduced APTT and PT values. HRG did not affect the changes in plasma levels of fibrinogen and antithrombin III (ATIII) levels in CLP mice (Fig. 3B).

Determination of blood cytokines 24 h after CLP revealed the marked increase in IL-6, TNF-α, and IL-10 levels in the CLP mice treated with PBS or HSA (Fig. 3C). HRG treatment almost completely inhibited the cytokine responses.

3.5. Effects of HRG on Morphology, Adhesion and Microcapillary Passage of Purified Human Neutrophils

To examine the effects of HRG on neutrophils in detail, we used human neutrophils purified from peripheral blood and labeled with calcein-AM and Hoechst33342. HRG (1 μM)-induced morphological changes were observed under a fluorescent microscope 60 min after incubation without a fixation procedure (Fig. 4A). The main features induced by HRG were the following: spherical shape change, loss of irregularity of shape, and shortening of the diameter. When compared with other media containing the same concentration of BSA, HSA, or fMLP, the spherical shape-inducing effects of HRG were evident (Fig. 4A and B). The adhesion of neutrophils to the plastic well was determined by counting the residual neutrophils after the wells were washed twice. The results clearly showed that the HRG-induced spherical shape were less adhesive to the plastic material (Fig. 4C). Quantification of HRG's spherical shape-inducing effects revealed HRG's concentration-dependent effects with the maximal response at 0.8 μM or above and EC_{50} around 0.1 μM (Fig. 4D). It took 15–30 min for HRG to induce a stable spherical shape from a freshly prepared cell suspension (Fig. S4 A). Moreover, the roundness of the completely flattened neutrophils was restored by the addition of HRG (1 μM) time-dependently, suggesting the reversibility of the shape-change response (Fig. S4B). The spherical structure-inducing effects of HRG were inhibited by the addition of rabbit polyclonal Ab against HRG but not by control IgG (Fig. 4E and F), confirming the specificity of HRG's effects. In addition to the inhibition of spherical shape, anti-HRG Ab antagonized HRG's inhibitory effect on neutrophil adhesion (Fig. 4G). The adhesion property of HRG-treated neutrophils on VECs (EA.hy926) was then examined (Fig. 4H–K). As shown in Fig. 4K, HRG significantly inhibited the adhesion of neutrophils on the EA.hy926 surface.

HRG's effects on the vertical transfer of neutrophils through micropores (5 μm diameter) were examined in a Boyden chamber. The results indicated that increasing concentrations of HRG as well as fMLP (1 μM) stimulated the transfer of neutrophils to the lower chamber (Fig. S5A). However, the chemotaxis-inducing activity to the horizontal direction was detected solely in fMLP and not in HRG. HRG did not only inhibit but also stimulated the chemotaxis induced by fMLP (Fig. S5B). Thus, the apparent transfer of neutrophils to the vertical direction may be ascribed to the decrease in diameter, the loss of microvilli, and gravity.

Scanning electron microscopic observation confirmed the loss of surface microvilli structures from neutrophils treated with HRG at least 15 min after the start of incubation (Fig. 5A and B). The microvilli on neutrophils were observed after incubation with buffer alone, BSA, HSA, and fMLP, as was the case with the washed neutrophils immediately after isolation (Fig. 5A and B). The cytochemical staining of G- and F-actin in neutrophils demonstrated that F-actin was dominant in HRG-treated neutrophils and that the HRG-induced spherical shape was accompanied by the F-actin ring formation beneath the plasma membrane of neutrophils (Fig. 5C). On the other hand, cytosolic G-actin was dominant in neutrophils treated with HBSS, BSA, and HSA (Fig. 5C). Few neutrophils had an F-actin ring under these conditions.

The passage of purified neutrophils through microcapillary slits (7.0 μm width, 4.5 μm depth) was evaluated by a MC-FAN under different conditions. Fig. 5D, E and Movie S3 show that neutrophils treated with HRG (1 μM) can pass microcapillaries more easily than can other treatment groups, in which the trapping of neutrophils with irregular shapes sometimes occurred before (red arrowheads) or on (white arrowheads) the microcapillary slits. HRG-treated neutrophils flowed through the slits much more smoothly in a teardrop shape (Fig. 5D and E; Movie S3). In contrast, the addition of anti-HRG mAb to whole blood retarded the passage of whole blood significantly, probably due to the trapping of leukocytes on the slits (Fig. 5F and G; Movie S4).

3.6. Pharmacological Analysis of HRG-inducing Signal Transduction in Neutrophils

Pretreatment with BAPTA for 30 min (50 μM) prevented HRG from inducing spherical shape formation (Fig. 6A). Determination of [Ca2 +]i after the prolonged incubation with HRG revealed that HRG induced time-dependent and very slow increases in [Ca2 +]i levels in neutrophils (Fig. 6B, C and S4C). Toxin B (100 ng/ml), a nonselective inhibitor of three small G proteins, Cdc42, Rac, and Rho, partially inhibits HRG's spherical-shape-inducing effects (Fig. 6D).

The production of ROS outside the neutrophils was determined at 15 min after the start of incubation by the detection of isoluminol chemiluminescence under different conditions (Fig. 6E). The ROS production levels in HRG (1 μM)-treated neutrophils were less than 5% the levels in the HBSS-, BSA-, and HSA-treated groups (Fig. 6E). The ROS production inside the neutrophils was determined by DCF fluorescence after incubation in the presence of HRG (1 μM) or other factors (Fig. 6F). Consistent with the extracellular ROS, ROS production inside

Fig. 5. *Relationship between neutrophil surface structure and passage through microcapillaries.* (*A* and *B*) The purified human neutrophils were incubated with reagents at 1 μM on a cover grass for 1 h at 37 °C. Scanning electron microscopic pictures of neutrophils were obtained. Time-dependent changes in the shapes (*B*). (*C*) The purified human neutrophils were incubated as in (*A*). The neutrophils were stained with Alexa Fluor 594-labeled phalloidin (red) for F-actin and Alexa Fluor 488-labeled DNase I (green) for G-actin. Cell nuclei were stained with DAPI (blue). Scale bars, 5 μm (*A* and *C*), 10 μm (*B*). (*D*) The purified human neutrophils were incubated with reagents at 1 μM for 60 min and then applied to a MC-FAN. Red arrowheads indicate the leukocytes attached to the upper chamber. White arrowheads indicate the leukocytes attached to the microcapillary entrance. (*E* and *G*) The time required for the passage of 100 μl neutrophil suspension through the MC-FAN was determined. $^{*}P < 0.05$, $^{\dagger\dagger}P < 0.01$, $^{\ddagger}P < 0.05$, and $^{\S\S\S}P < 0.001$ *vs.* HBSS, BSA, HSA, and fMLP, respectively (*E*). $^{*}P < 0.05$ *vs.* IgG control (*G*). (*F*) The anti-coagulated whole blood treated with anti-HRG Ab or control IgG was applied to the MC-FAN. White arrowhead indicates the leukocyte attached on the microcapillary entrance. The results shown are the means ± SEM of five experiments (*E* and *G*).

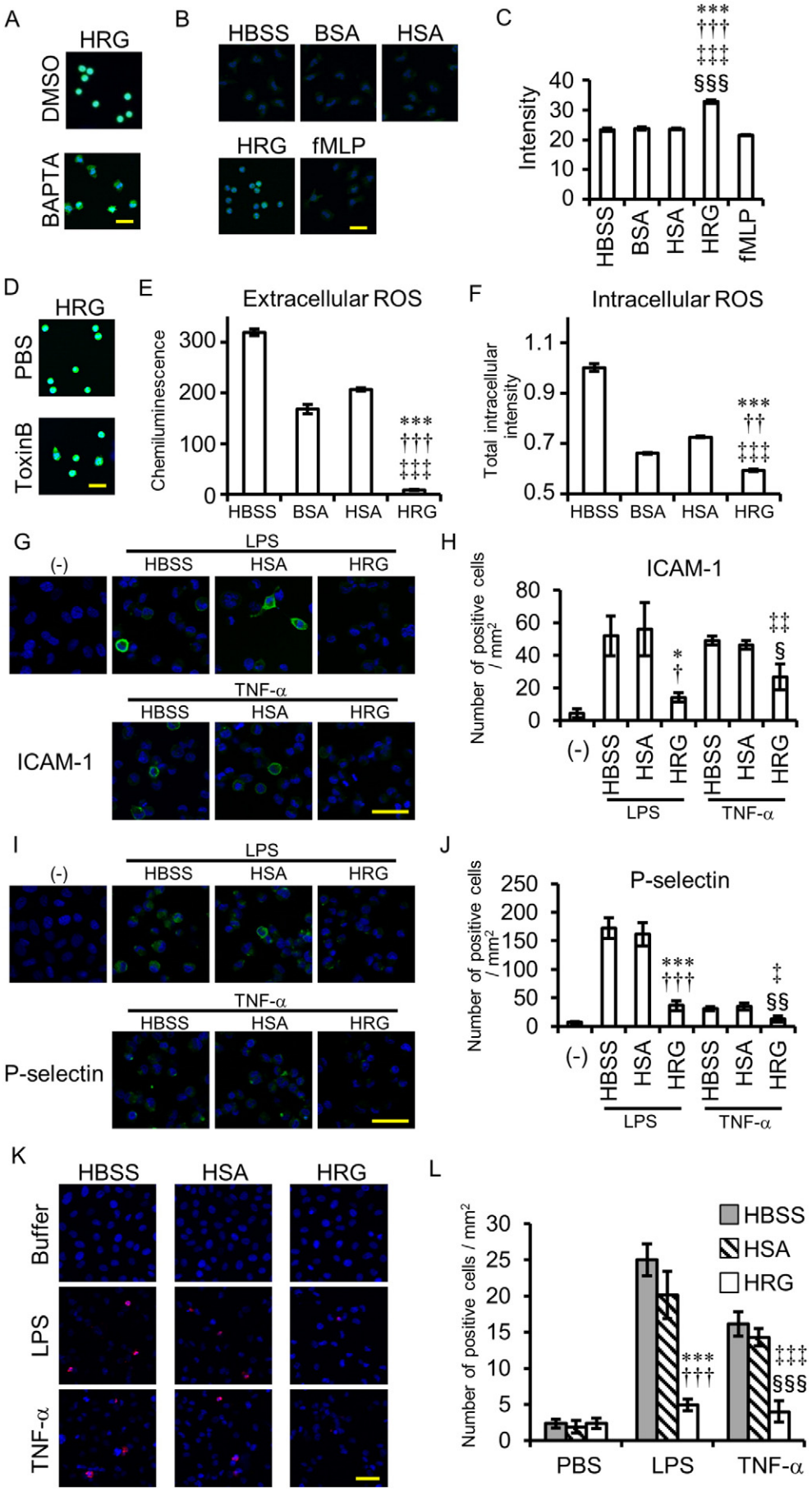
A
HRG
DMSO
BAPTA
B
HBSS
BSA
HSA
HRG
fMLP
C
Intensity
HBSS
BSA
HSA
HRG
fMLP
D
HRG
PBS
ToxinB
E
Extracellular ROS
Chemiluminescence
F
Intracellular ROS
Total intracellular intensity
G
LPS
(-)
HBSS
HSA
HRG
TNF-α
ICAM-1
H
ICAM-1
Number of positive cells / mm²
LPS
TNF-α
I
P-selectin
J
P-selectin
K
Buffer
LPS
TNF-α
L
PBS
LPS
TNF-α

the cells was lower in HRG-treated neutrophils than in any of the other groups (Fig. 6F). Although HRG did not affect the expression of CD11b, CD62L, CD162 on neutrophils in resting as well as agonist (C5a, IL-8, and fMLP)-stimulated condition, HRG slightly inhibited the expression of activated form of CD11b, irrespective of the presence of agonists (Fig. S6). These results as a whole indicated that HRG-induced spherical shape changes were accompanied by functional alterations of the neutrophils, including changes in ROS production, adhesion to VECs, and passage through microcapillaries.

3.7. Effects of HRG on LPS- or TNF-α-induced Expression of Adhesion Molecules and Cell Death in VECs

VECs must be activated or lesioned under septic condition. Therefore, we determined the effects of HRG on VECs (EA.hy926), and especially focused on adhesion molecule expression and cell death. As shown in Figs. 6G–J and S7, HRG (1 μM) inhibited LPS (10 ng/ml)- or TNF-α (10 ng/ml)-induced expression of ICAM-1 and P-selectin. Also, HRG (1 μM) strongly inhibited the endothelial cell death induced by both LPS and TNF-α (Figs. 6K, L and S7), suggesting a protective role of HRG against endothelial injury.

4. Discussion

In the present study, we clearly showed a novel and important role of HRG in controlling the shape, adhesiveness, passage, and basal ROS-producing activity of neutrophils. No plasma protein has ever been reported to have such activity. Judging from the plasma HRG levels (around 1 μM) in healthy human (Poon et al., 2011; Saigo et al., 1990), the effects of HRG on neutrophil shape in the circulation under normal condition are speculated to be maximal. A marked decrease in plasma levels of HRG in septic conditions due to rapid reduction in HRG gene expression, deposition of HRG on immunothrombi and degradation of HRG by thrombin (Fig 1E and F; Figs. S1G, S2 A and S2B) may lead to increased adhesion of neutrophils to VECs and retardation of neutrophil passage in the microvasculature demonstrated by *in vivo* imaging and *in vitro* experiments; the changes are associated with the enhancement of ROS production. Thus, the neutrophil shape maintained by HRG should be suitable for their passage through the capillary vessels, sustaining rheological stability, and preventing unnecessary activaton of VECs. The spherical shape probably minimizes the surface attachment area of neutrophils to VECs and reduces physical contact between neutrophils and endothelial cells in the microvasculature, easing the passage of neutrophils through capillary vessels as observed by *in vivo* imaging of circulating neutrophils in CLP mice treated with HRG. In addition, it was revealed that HRG slightly inhibited the expression of activated but not inactivated form of CD11b, irrespective of the presence of neutrophil activation agonists. This effect of HRG may also limit the unnecessary tight interaction between circulating neutrophils and VECs. In contrast, the deformed neutrophils in septic condition sometimes occupy the flow of microcirculation by forming a cell cluster, implying enhanced interaction between deformed neutrophils and VECs or deformed cells themselves. This attachment pattern seems quite different from that observed during the migration of neutrophils infiltrating inflamed sites (Amulic et al., 2012; DiStasi and Ley, 2009; Phillipson and Kubes, 2011).

Immunohistochemical analysis of septic ARDS in CLP mice clearly showed the existence of immunothrombi in lung vasculatures. The marked inhibitory effects of HRG on immunothrombosis in pulmonary vasculatures (Fig. 2C and E) were presumably due to suppression of initial neutrophil attachment by keeping morphological and functional quiescence of circulating neutrophils and inhibition of the formation of fibrin clot on neutrophil and platelets. In addition, almost complete inhibition of the increase in plasma IL-6 and TNF-α by HRG administration could contribute to cancellation of activation of VECs that facilitates immunothrombosis. The finding that HRG antagonized the pro-DIC state together with the anti-immunothrombotic effects as well as strong inhibition of lung inflammation implies that HRG administration suppressed the major and fatal responses in sepsis; DIC, multiple organ failure due to microthrombus formation, and severe inflammatory injuries in plural organs. It was reported that NET formation (Brinkmann et al., 2004; Yipp and Kubes, 2013) was involved in different types of immunothrombosis. In the present model, we confirmed NETosis occurring in the lung vasculatures leading to immunothrombosis (Fig. 2F and G).

The HRG-induced shape change of neutrophils associated with polymerization of actin beneath the plasma membrane may be accompanied by the activation of Rho family signaling pathway(s) sensitive to Toxin B and the regulation of cytosolic calcium judging from the antagonizing effects of BAPTA and the time-dependent increase in intracellular calcium by HRG. Further works are necessary to clarify upstream signaling mechanisms of HRG action including identification of receptor molecule involved.

C5a, IL-8, and fMLP induced the expression of CD11b and CD162 on the neutrophil surface and shed off CD62L, as detected by FACS (Fig. S6). HRG did not influence the basal and agonist-induced changes in adhesion molecules on the neutrophil surface except for activated form of CD11b (Fig. S6). Since HRG did not influence the expression of PSGL-1 and Mac-1 induced by IL-8, C5a, and fMLP, HRG was speculated not to inhibit the agonists-induced facilitation of neutrophil migration to the destination. This speculation was supported by the present finding that there were no differences in the total number of infiltrating neutrophils in the peritoneal cavity between HRG-treated and control CLP mice (Fig. S1F) and HRG neither stimulated nor inhibited migration to horizontal direction in chemotaxis assay (Fig. S5). Therefore, it is possible that HRG does not interfere with neutrophil activation and migration of neutrophils which are responsible for the recruitment of neutrophils into inflamed sites while playing a role in maintaining the basal state of circulating neutrophils. In contrast, HRG concentration dependently antagonized agonist-induced morphological changes and *vice versa* (Fig. S8).

Excess activation and even lesion of VECs represent the disorder of septic condition (Opal and van der Poll, 2015). The inhibition of expression of ICAM-1 and P-selectin on VECs induced by LPS or TNF-α *in vitro* by the addition of HRG (1 μM) strongly suggested that physiological concentration of HRG in the circulation constantly suppresses the activation of VECs. Furthermore, HRG appeared to play a protective role against endothelial cell death induced by LPS and TNF-α. Thus, it was

Fig. 6. *Analysis of signal transduction pathways for HRG's effects on neutrophils and effects of HRG on VECs.* (*A*) The neutrophils were loaded with BAPTA-AM (50 μM) or DMSO for 20 min and incubated with HRG (1 μM) for 1 h. (*B*) The neutrophils were loaded with Fluo-4-AM for 20 min and incubated with reagents at 1 μM for 1 h. Intracellular calcium was monitored by Fluo-4 fluorescence. (*C*) The average of Fluo-4 fluorescence intensity was calculated by In Cell Analyzer. $^{***}P < 0.001$, $^{\dagger\dagger\dagger}P < 0.001$, $^{\ddagger\ddagger\ddagger}P < 0.001$, and $^{\S\S\S}P < 0.001$ *vs.* HBSS, BSA, HSA, and fMLP, respectively. (*D*) The neutrophils were preincubated with Toxin B (100 ng/ml) or PBS for 1.5 h and then incubated with HRG (1 μM) for 1 h. (*E*) The neutrophils were incubated with reagents at 1 μM for 15 min, and the ROS produced extracellularly was determined using isoluminol as a substrate. The chemiluminescence in the medium was determined by a plate reader. $^{***}P < 0.001$, $^{\dagger\dagger\dagger}P < 0.001$, and $^{\ddagger\ddagger\ddagger}P < 0.001$ *vs.* HBSS, BSA, and HSA, respectively. (*F*) The neutrophils were loaded with CM-H_2DCFDA for 20 min and incubated with reagents at 1 μM for 1 h. The fluorescence of DCF was detected by the In Cell Analyzer. $^{***}P < 0.001$, $^{\dagger\dagger}P < 0.01$, and $^{\ddagger\ddagger\ddagger}P < 0.001$ *vs.* HBSS, BSA, and HSA, respectively. (*G–K*) Monolayer of EA.hy926 cells were stimulated with LPS (10 ng/ml) or TNF-α (10 ng/ml) in the presence of HBSS, HSA, or HRG for 30 min at 37 °C. The cells were stained by anti-human ICAM-1 Ab (*G* and *H*), anti-human P-selectin Ab (*I* and *J*) or anti-phosphatidylserine Ab (*K* and *L*), for 25 min at 4 °C. (*G–J*) (−) is no stimulated-sample. (*H*, *J*, and *L*) ICAM-1 (*H*), P-selectin (*I*) or phosphatidylserine (*J*) -positive cells were counted in each group. $^{*}P < 0.05$, $^{***}P < 0.001$ *vs.* LPS + HBSS. $^{\dagger}P < 0.05$, $^{\dagger\dagger\dagger}P < 0.001$ *vs.* LPS + HSA. $^{\ddagger}P < 0.05$, $^{\ddagger\ddagger}P < 0.01$, $^{\ddagger\ddagger\ddagger}P < 0.001$ *vs.* TNF-α + HBSS. $^{\S}P < 0.05$, $^{\S\S}P < 0.01$, $^{\S\S\S}P < 0.001$ *vs.* TNF-α + HSA. The results shown are the means ± SEM of three experiments (*C*, *E*, and *F*), four fields (*H* and *J*) or six fields (*L*). Scale bars, 20 μm (*A*, *B*, and *D*), 50 μm (*G*, *I*, and *K*).

concluded that HRG is a crucial regulatory factor of VEC function. We should mention that HRG may exert its effects on mononuclear phagocytes in septic condition in addition to neutrophils and VECs because the binding of HRG to mononuclear phagocytes was reported (Tugues et al., 2014) and phenotype change of macrophages by HRG was observed in cancer (Rolny et al., 2011).

Taken together, the results in the present study strongly suggested that the decrease in plasma HRG constitutes the fundamental pathway for septic pathogenesis. The supplementary treatment of CLP mice with HRG may simultaneously improve complex and multiple aspects of the serious disorders found in septic conditions: the uncontrolled activation of circulating neutrophils, the activation and lesion of VECs, the immunothrombosis, cytokine overproduction, and the disorder of coagulation and fibrinolysis cascades. Supplementary therapy with HRG may provide a novel strategy for the treatment of septic patients (Ward, 2012; Opal et al., 2013; Ranieri et al., 2012; Rice et al., 2010; Russell, 2006) although there might be a therapeutic time window for the treatment.

Supplementary data to this article can be found online at http://dx.doi.org/10.1016/j.ebiom.2016.06.003.

Conflicts of Interest

The authors declare that they have no conflicts of interest.

Author Contributions

H.W., S.M., H.T., and M.N. planned the study; H.W., S.M., Y.M., and M.S. performed the experiments using purified human neutrophils; Y.G. performed the experiments using vascular endothelial cells; H.W., K.L., H.T., and K.T. performed the sepsis mice experiments; A.O. and T.Y. analyzed neutrophil shape and histological features, respectively; K.K. and H.M determined the plasma HRG in septic patients; H.W., S.M., and M.N. wrote the manuscript.

Acknowledgments

This work was supported by grants from Scientific Research from the Ministry of Health, Labour, and Welfare of Japan (WA2F2547, WA2F2601), the Japan Agency for Medical Research and Development, AMED (15lk0201014h0003), the Japan Society for the Promotion of Science (JSPS No. 2567046405, 15H0468617), and Secom Science and Technology Foundation to M.N. and from the Hokuto Foundation for Bioscience to H.W. We thank M. Sato, M. Narasaki, and H. Nakamura for their technical assistance. Human fresh frozen plasma was kindly provided by the Japanese Red Cross Society.

References

Alves-Filho, J.C., de Freitas, A., Spiller, F., Souto, F.O., Cunha, F.Q., 2008. The role of neutrophils in severe sepsis. Shock 1, 3–9.
Amulic, B., Cazalet, C., Hayes, G.L., Metzler, K.D., Zychlinsky, A., 2012. Neutrophil function: from mechanisms to disease. Annu. Rev. Immunol. 30, 459–489.
Aziz, M., Jacob, A., Yang, W.L., Matsuda, A., Wang, P., 2013. Current trends in inflammatory and immunomodulatory mediators in sepsis. J. Leukoc. Biol. 93, 329–342.
Borza, D.B., Tatum, F.M., Morgan, W.T., 1996. Domain structure and conformation of histidine-proline-rich glycoprotein. Biochemistry 35, 1925–1934.
Bosshart, H., Heinzelmann, M., 2003. Endotoxin-neutralizing effects of histidine-rich peptides. FEBS Lett. 553, 135–140.
Brinkmann, V., Reichard, U., Goosmann, C., Fauler, B., Uhlemann, Y., Weiss, D.S., Weinrauch, Y., Zychlinsky, A., 2004. Neutrophil extracellular traps kill bacteria. Science 303, 1532–1535.
Dellinger, R.P., Levy, M.M., Rhodes, A., Annane, D., Gerlach, H., Opal, S.M., Sevransky, J.E., Sprung, C.L., Douglas, I.S., Jaeschke, R., et al., 2012. Surviving sepsis campaign: international guidelines for management of severe sepsis and septic shock: 2012. Crit. Care Med. 41, 580–637.
DiStasi, M.R., Ley, K., 2009. Opening the flood-gates: how neutrophil-endothelial interactions regulate permeability. Trends Immunol. 30, 547–556.
Doñate, F., Juarez, J.C., Guan, X., Shipulina, N.V., Plunkett, M.L., Tel-Tsur, Z., Shaw, D.E., Morgan, W.T., Mazar, A.P., 2004. Peptides derived from the histidine-proline domain of the histidine-proline-rich glycoprotein bind to tropomyosin and have antiangiogenic and antitumor activities. Cancer Res. 64, 5812–5817.
Engelmann, B., Massberg, S., 2013. Thrombosis as an intravascular effector of innate immunity. Nat. Rev. Immunol. 13, 34–45.
Gorgani, N.N., Parish, C.R., Easterbrook, Smith, S.B., Altin, J.G., 1997. Histidine-rich glycoprotein binds to human IgG and C1q and inhibits the formation of insoluble immune complexes. Biochemistry 36, 6653–6662.
Grommes, J., Soehnlein, O., 2011. Contribution of neutrophils to acute lung injury. Mol. Med. 17, 293–307.
Hotchkiss, R.S., Monneret, G., Payen, D., 2013. Immunosuppression in sepsis: a novel understanding of the disorder and a new therapeutic approach. Lancet Infect. Dis. 13, 260–268.
Juarez, J.C., Guan, X., Shipulina, N.V., Plunkett, M.L., Parry, G.C., Shaw, D.E., Zhang, J.C., Rabbani, S.A., McCrae, K.R., Mazar, A.P., et al., 2002. Histidine-proline-rich glycoprotein has potent antiangiogenic activity mediated through the histidine-proline-rich domain. Cancer Res. 62, 5344–5350.
Kacprzyk, L., Rydengård, V., Mörgelin, M., Davoudi, M., Pasupuleti, M., Malmsten, M., Schmidtchen, A., 2007. Antimicrobial activity of histidine-rich peptides is dependent on acidic conditions. Biochim. Biophys. Acta 1768, 2667–2680.
Koide, T., Foster, D., Yoshitake, S., Davie, E.W., 1986. Amino acid sequence of human histidine-rich glycoprotein derived from the nucleotide sequence of its cDNA. Biochemistry 25, 2220–2225.
Leung, L.L., 1986. Interaction of histidine-rich glycoprotein with fibrinogen and fibrin. J. Clin. Invest. 77, 1305–1311.
Levy, M.M., Fink, M.P., Marshall, J.C., Abraham, E., Angus, D., Cook, D., Cohen, J., Opal, S.M., Vincent, J.L., Ramsay, G., 2003. 2001 SCCM/ESICM/ACCP/ATS/SIS International Sepsis Definitions Conference. Crit. Care Med. 31, 1250–1256.
Lijnen, H.R., Hoylaerts, M., Collen, D., 1983. Heparin binding properties of human histidine-rich glycoprotein. Mechanism and role in the neutralization of heparin in plasma. J. Biol. Chem. 258, 3803–3808.
Matthay, M.A., Zemans, R.L., 2011. The acute respiratory distress syndrome: pathogenesis and treatment. Annu. Rev. Pathol. 6, 147–163.
Moreland, J.G., Bailey, G., Nauseef, W.M., Weiss, J.P., 2004. Organism-specific neutrophil-endothelial cell interactions in response to *Escherichia coli*, *Streptococcus pneumoniae*, and *Staphylococcus aureus*. J. Immunol. 172, 426–432.
Morgan, W.T., 1985. The histidine-rich glycoprotein of serum has a domain rich in histidine, proline, and glycine that binds heme and metals. Biochemistry 24, 1496–1501.
Mori, S., Takahashi, H.K., Yamaoka, K., Okamoto, M., Nishibori, M., 2003. High affinity binding of serum histidine-rich glycoprotein to nickel-nitrilotriacetic acid: the application to microquantification. Life Sci. 73, 93–102.
Opal, S.M., van der Poll, T., 2015. Endothelial barrier dysfunction in septic shock. J. Intern. Med. 277, 277–293.
Opal, S.M., Laterre, P.F., Francois, B., LaRosa, S.P., Angus, D.C., Mira, J.P., Wittebole, X., Dugernier, T., Perrotin, D., Tidswell, M., et al., 2013. Effect of Eritoran, an antagonist of MD2-TLR4, on mortality in patients with severe sepsis. JAMA 309, 1154–1162.
Peterson, C.B., Morgan, W.T., Blackburn, M.N., 1987. Histidine-rich glycoprotein modulation of the anticoagulant activity of heparin. Evidence for a mechanism involving competition with both antithrombin and thrombin for heparin binding. J. Biol. Chem. 262, 7567–7574.
Phillipson, M., Kubes, P., 2011. The neutrophil in vascular inflammation. Nat. Med. 17, 1381–1390.
Piccinini, A.M., Midwood, K.S., 2010. DAMPening inflammation by modulating TLR signalling. Mediat. Inflamm. 2010, 1–21.
Poon, I.K., Hulett, M.D., Parish, C.R., 2010. Histidine-rich glycoprotein is a novel plasma pattern recognition molecule that recruits IgG to facilitate necrotic cell clearance via FcgammaRI on phagocytes. Blood 115, 2473–2482.
Poon, I.K., Patel, K.K., Davis, D.S., Parish, C.R., Hulett, M.D., 2011. Histidine-rich glycoprotein: the Swiss Army knife of mammalian plasma. Blood 117, 2093–2101.
Ranieri, V.M., Thompson, B.T., Barie, P.S., Dhainaut, J.F., Douglas, I.S., Finfer, S., Gårdlund, B., Marshall, J.C., Rhodes, A., Artigas, A., et al., 2012. Drotrecogin alfa (activated) in adults with septic shock. N. Engl. J. Med. 366, 2055–2064.
Rice, T.W., Wheeler, A.P., Bernard, G.R., Vincent, J.L., Angus, D.C., Aikawa, N., Demeyer, I., Sainati, S., Amlot, N., Cao, C., et al., 2010. A randomized, double-blind, placebo-controlled trial of TAK-242 for the treatment of severe sepsis. Crit. Care Med. 38, 1685–1694.
Rolny, C., Mazzone, M., Tugues, S., Laoui, D., Johansson, I., Coulon, C., Squadrito, M.L., Segura, I., Li, X., Knevels, E., et al., 2011. HRG inhibits tumor growth and metastasis by inducing macrophage polarization and vessel normalization through downregulation of PlGF. Cancer Cell 19, 31–44.
Russell, J.A., 2006. Management of sepsis. N. Engl. J. Med. 355, 1699–1713.
Rydengård, V., Olsson, A.K., Mörgelin, M., Schmidtchen, A., 2007. Histidine-rich glycoprotein exerts antibacterial activity. FEBS J. 274, 377–389.
Rydengård, V., Shannon, O., Lundqvist, K., Kacprzyk, L., Chalupka, A., Olsson, A.K., Mörgelin, M., Jahnen-Dechent, W., Malmsten, M., Schmidtchen, A., 2008. Histidine-rich glycoprotein protects from systemic Candida infection. PLoS Pathog. 4, e1000116.
Saigo, K., Yoshida, A., Ryo, R., Yamaguchi, N., Leung, L.L., 1990. Histidine-rich glycoprotein as a negative acute phase reactant. Am. J. Hematol. 34, 149–150.
Salomão, R., Martins, P.S., Brunialti, M.K., Fernandes, Mda, L., Martos, L.S., Mendes, M.E., Gomes, N.E., Rigato, O., 2008. TLR signaling pathway in patients with sepsis. Shock 30, 73–77.
Semeraro, N., Ammollo, C.T., Semeraro, F., Colucci, M., 2012. Sepsis, thrombosis and organ dysfunction. Thromb. Res. 129, 290–295.
Shannon, O., Rydengård, V., Schmidtchen, A., Mörgelin, M., Alm, P., Sørensen, O.E., Björck, L., 2010. Histidine-rich glycoprotein promotes bacterial entrapment in clots and decreases mortality in a mouse model of sepsis. Blood 116, 2365–2372.

Silverstein, R.L., Leung, L.L., Harpel, P.C., Nachman, R.L., 1985. Platelet thrombospondin forms a trimolecular complex with plasminogen and histidine-rich glycoprotein. J. Clin. Invest. 75, 2065–2073.
Sudom, K., Turrin, N.P., Hayley, S., Anisman, H., 2004. Influence of chronic interleukin-2 infusion and stressors on sickness behaviors and neurochemical change in mice. Neuroimmunomodulation 11, 341–350.
Tugues, S., Roche, F., Noguer, O., Orlova, A., Bhoi, S., Padhan, N., Akerud, P., Honjo, S., Selvaraju, R.K., Mazzone, M., et al., 2014. Histidine-rich glycoprotein uptake and turnover is mediated by mononuclear phagocytes. PLoS One 9, e107483.
Wake, H., Mori, S., Liu, K., Takahashi, H.K., Nishibori, M., 2009. Histidine-rich glycoprotein inhibited high mobility group box 1 in complex with heparin-induced angiogenesis in matrigel plug assay. Eur. J. Pharmacol. 623, 89–95.
Ward, P.A., 2012. New approaches to the study of sepsis. EMBO Mol. Med. 4, 1234–1243.
Williams, M.R., Azcutia, V., Newton, G., Alcaide, P., Luscinskas, F.W., 2011. Emerging mechanisms of neutrophil recruitment across endothelium. Trends Immunol. 32, 461–469.
Yipp, B.G., Kubes, P., 2013. NETosis: how vital is it? Blood 122, 2784–2794.